We are IntechOpen,
the world's leading publisher of
Open Access books
Built by scientists, for scientists

4,800
Open access books available

122,000
International authors and editors

135M
Downloads

154
Countries delivered to

Our authors are among the

TOP 1%
most cited scientists

12.2%
Contributors from top 500 universities

CLARIVATE ANALYTICS

BOOK
CITATION
INDEX

INDEXED

WEB OF SCIENCE™

Selection of our books indexed in the Book Citation Index
in Web of Science™ Core Collection (BKCI)

Interested in publishing with us?
Contact book.department@intechopen.com

Numbers displayed above are based on latest data collected.
For more information visit www.intechopen.com

All-Optical Signal Processing for High Spectral Efficiency (SE) Optical Communication

Y. Ben Ezra, B.I. Lembrikov, Avi Zadok, Ran Halifa and D. Brodeski

Additional information is available at the end of the chapter

1. Introduction

All-optical signal processing is essential for optical communication systems transmitting high speed data signals. All-optical wavelength conversion (WC), pulse generation, orthogonal frequency-division multiplexing (OFDM), demultiplexing, regeneration, modulation format conversion are the important signal processing functions. The limiting factors in the existing ultra long haul optical communication systems are spectral efficiency (SE), fiber attenuation, insertion losses, chromatic dispersion, polarization mode dispersion (PMD), and the optical fiber nonlinearity [1]-[4]. Optical communication systems can be divided into two groups. In the first group, an electrical signal modulates the intensity of an optical carrier inside the optical transmitter, the modulated optical signal is transmitted through the optical fiber and converted to the original electrical signal by an optical receiver [1]. Such a scheme is called an intensity modulation with direct detection (IM/DD) [1], [5]. In the second group, information is transmitted by modulation of the optical carrier frequency or phase, and then the modulated optical signal can be linearly down-converted to a baseband electrical signal by heterodyne or homodyne detection [1], [5]. The phase coherence of the optical carrier is essential for the realization of the second group called coherent optical communication systems [1].

Coherent optical communication systems possess the following advantages with respect to IM/DD systems: (i) the shot-noise limited receiver can be achieved with a sufficient local oscillator (LO) power; (ii) the frequency resolution at the intermediate frequency (IF) or baseband stage is high enough in order to separate close wavelength-division multiplexed (WDM) channels in the electric domain; (iii) the phase detection improves the receiver sensitivity compared with IM/DD systems; (iv) the multilevel modulation formats can be introduced into optical communications by using phase modulation [5].

The rapid development of digital communication and digital signal processing (DSP) caused by the necessity of high SE and, at the same time, by the advance of the high-speed

electronics required advanced modulation, coding and digital equalization [6]. Recently, coherent optical communications attracted a large interest due to the feasibility of the high SE, the large bandwidth and multilevel modulation formats [5]. Coherent optical systems using multilevel modulation formats can increase SE up to M b/s/Hz where M is the number of bits per symbol for a given modulation format [5].

Coherent optical OFDM (CO-OFDM) has been recently proposed in order to increase receiver sensitivity, SE, and especially, provide the dispersion compensation at high data transmission rates tending to 100Gb/s [3], [4], [7], [8]. Generally, OFDM is a kind of multicarrier modulation (MCM) in which the data information is carried over many lower rate subcarriers [4]. In OFDM spectra of individual subcarriers overlap, but due to the orthogonality, the subcarriers can be demodulated without interference and without analog filtering for the received subcarrier separation [7]. The signal processing in the OFDM system can be carried out by using the Fast Fourier Transform (FFT)/Inverse Fast Fourier Transform (IFFT) [3], [4], [7]. In CO-OFDM systems the digital signal processing is used in order to mitigate the channel dispersion, nonlinearity and different types of noise.

CO-OFDM system combines the following advantages of coherent detection and OFDM modulation essential for the high-speed optical fiber communication systems: (i) in CO-OFDM systems, chromatic dispersion and PMD can be mitigated; (ii) the SE of CO-OFDM systems is high due to the partial overlapping of OFDM sub-carrier spectra; (iii) linearity in radio frequency (RF)-to-optical (RTO) up-conversion and optical-to-RF (OTR) down-conversion; (iv) the electrical bandwidth requirements for the CO-OFDM transceiver can be greatly reduced by using direct up/down conversion which results in the low cost of the high-speed electronic circuits [3], [4], [8]. Recently, all-optical FFT scheme enabling Tbit/s real-time signal processing has been proposed [9]. The method based on only passive optical components realizes the highest speed signal processing without the power consumption where electronics cannot be used. This approach combines the advantages of the electronic high precision processing of the low bit rates and the optical processing of high bit rates [9].

However, OFDM is characterized by the inter-symbol-interference (ISI) and inter-carrier-interference (ICI) caused by a large number of subcarriers [4]. In the RF systems ISI is mainly due to multipath channel delay spread [10], [11] and ICI is mainly due to the carrier frequency offset [12]. In the case of CO-OFDM, ISI and ICI are caused by channel chromatic dispersion and PMD [3], [4]. A so-called cyclic prefix (CP), i.e. the cyclic extension of the OFDM waveform into the guard interval (GI) Δ_G, has been proposed in order to prevent ISI and ICI [4]. If the GI is long enough to contain the intersymbol transition, then the remaining part of the OFDM symbol satisfies the orthogonality condition and receiver cross-talk occurs only within GI [9]. The addition of CP requires an increase of a bandwidth and sampling rate of analog-to-digital converter (ADC) and digital-to-analog converter (DAC). CP appeared to be an easily recognizable feature of an OFDM system making the signal vulnerable to interception by surveillance receiver [10]. The elimination of CP reduces the probability of interception and improves SE [10].

The need for CP can be avoided if the wavelet packet transform (WPT) is used in CO-OFDM systems instead of discrete Fourier Transform (DFT) and inverse DFT (IDFT) [13]. The sinusoidal functions are infinitely long in the time domain while wavelets have finite length being localized in time and in frequency domains [13]. Wavelet signal analysis can be a base for an effective computational algorithm which is faster and simpler than FFT [14]. Wavelets have been used in optical communications for time-frequency multiplexing and ultrafast image transmission [14]. A signal may be expanded in an orthogonal set of wavelet packets (WPs) as the basis functions, each channel occupies a wavelet packet (WP), and IDWPT/ DWPT are used at the transmitter and receiver, respectively [13].

In this chapter, we consider the CO-OFDM based on WPT and its influence on the optical communication network performance. The chapter is constructed as follows. In Section 2, we review the coherent optical communication systems. In Section 3, we discuss high SE CO-OFDM system. In Section 4, we discuss the OFDM based on WPT and present the original results for the WPT-OFDM system performance. In Section 5, we present the original results concerning the simulations of the structure and operation mode of the novel passive components for all-optical signal processing based on Si-on-insulator (SOI) structure, and a novel hierarchical architecture of the 1Tb/s transmission system based on WPT-OFDM [15]. In Section 6, conclusions are presented.

2. Coherent optical communication systems

The number of publications concerning the coherent optical communications is enormous. In this section, we can only relate to a limited number of the fundamental works concerning the concept of the coherent detection and the modulation formats used in digital communication system since these topics are related to high SE CO-OFDM systems.

The most advanced detection method is coherent detection based on the recovery of the full electric field containing both amplitude and phase information [16]. The concept of the coherent detection is to combine in a receiver the modulated optical signal with a continuous wave (CW) optical field generated by a narrow linewidth laser, or local oscillator (LO) before the photodetector (PD) [1]. Coherent detection requires the carrier synchronization with respect to LO that serves as an absolute phase reference [16]. For this purpose, optical systems can use two types of the phase-locked loops (PLLs): (i) an optical PLL (OPLL) that synchronizes the frequency and phase of the LO laser with the transmitter laser; (ii) an electrical PLL where down-conversion with a free-running LO laser is followed by a second-stage demodulation by an electrical voltage controlled oscillator (VCO) with the synchronized frequency and phase [16].

The basic component of coherent optical systems is a coherent optical receiver [1], [5]. Its block diagram is shown in Figure 1 [5].

The electric fields $E_s(t)$ and $E_{LO}(t)$ of the received optical signal and LO, respectively, are given by [5]

$$E_s(t) = A_s(t)\exp\left[j\left(\omega_0 t + \phi_s\right)\right]; E_{LO}(t) = A_{LO}\exp\left[j\left(\omega_{LO}t + \phi_{LO}\right)\right] \tag{1}$$
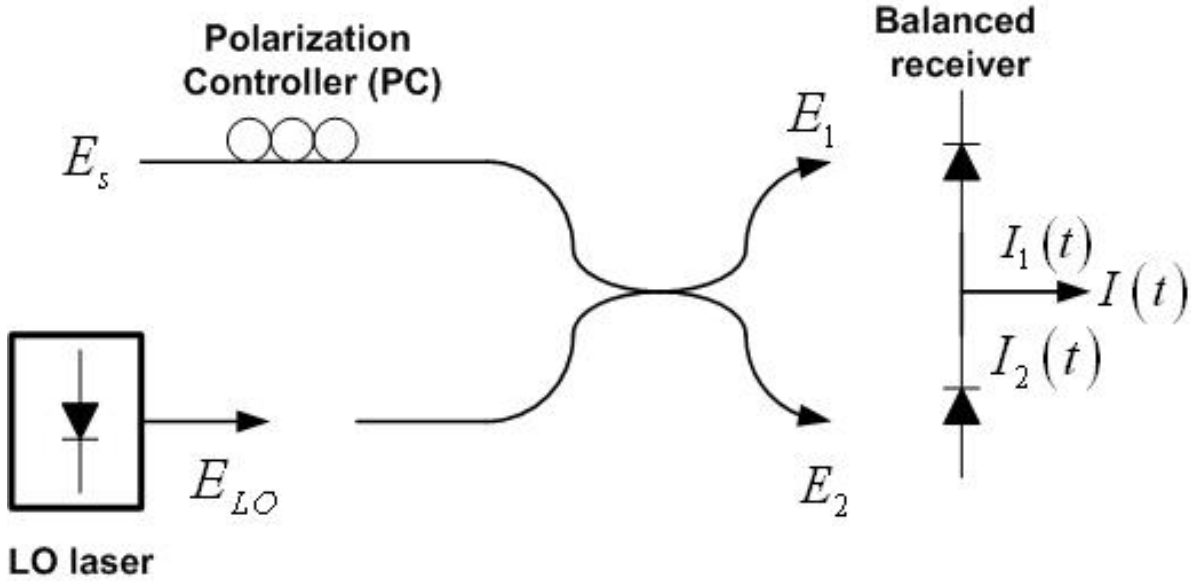
Figure 1. Block diagram of the coherent receiver

where $A_s(t), A_{LO}, \omega_0, \omega_{LO}, \phi_s, \phi_{LO}$ are the amplitudes, frequencies and phases of the received optical signal and LO, respectively. A 3db optical coupler (OC) is used that adds a π phase shift to either the signal field or the LO field between the two output ports. When the signal and LO fields are co-polarized, the electric fields $E_{1,2}$ incident on the upper and lower diodes are given by, respectively.

$$E_{1,2} = \frac{1}{\sqrt{2}}\left[E_s(t) \pm E_{LO}(t)\right]$$ (2)

The output photocurrents $I_{1,2}(t)$ are given by, respectively [5]

$$I_{1,2}(t) = \frac{R}{2}\left\{P_s + P_{LO} \pm 2\sqrt{P_s P_{LO}}\cos\left(\omega_{IF}t + \phi_s - \phi_{LO}\right)\right\}$$ (3)

where $P_s = A_s^2(t)/2, P_{LO} = A_{LO}^2/2, \omega_{IF} = \omega_0 - \omega_{LO}$ is IF, $R = e\eta_q/(\hbar\omega_0)$ is the detector responsivity, e is the electron charge, η_q is the PD quantum efficiency, $\hbar = h/2\pi, h$ is the Planck's constant. The sum frequency component is neglected since it is averaged out to zero over the bandwidth of PD. Balanced detection is used in order to suppress the DC component and maximize the signal photocurrent $I(t)$ at the balanced detector output given by [5]

$$I(t) = 2R\sqrt{P_s(t)P_{LO}}\cos\left(\omega_{IF}t + \phi_s - \phi_{LO}\right)$$ (4)

Eq. (4) demonstrates the main advantage of the coherent detection as compared to the direct detection. The photocurrent $I(t)$ contains explicitly the signal phase ϕ_s making possible to transmit information by modulating the phase or frequency of the carrier signal [1], [5]. There are two cases of the coherent detection: (i) the heterodyne detection when the signal

carrier frequency ω_0 and the LO frequency ω_{LO} are different, and $f_{IF} = \omega_{IF}/(2\pi) \sim 1GHz$; (ii) the homodyne detection when the signal carrier frequency ω_0 and the LO frequency ω_{LO} coincide, and IF $\omega_{IF} = 0$ [1]. In the heterodyne detection case, eq. (4) describes the output photocurrent. Typically, the LO power is much larger than the received signal power: $P_{LO} \gg P_s$, and LO amplifies the received signal improving signal-to-noise ratio (SNR) [1]. In the case of the heterodyne detection, the optical signal is demodulated in two stages: it is first down-converted to IF and then to the baseband [1]. The output photocurrent $I(t)$ (4) then takes the form.

$$I(t) = 2R\sqrt{P_s(t)P_{LO}}\cos(\phi_s - \phi_{LO}) \tag{5}$$

Similarly, the increase of the average electrical power up to 20dB can occur in the case of the homodyne detection. If additionally, the LO phase is locked to the signal phase so that $\phi_s - \phi_{LO} = 0$ eq. (5) takes the form [1].

$$I(t) = 2R\sqrt{P_s(t)P_{LO}} \tag{6}$$

The phase difference $\phi_s - \phi_{LO}$ can be kept constant by using an OPLL. However, the implementation of OPLL makes the design of optical homodyne receivers a comparatively complicated problem [1], [5].

The coherent detection allows the greatest flexibility in modulation formats, since information can be encoded by modulating the amplitude, the phase, or the frequency of an optical carrier as it is seen from equations (1)-(6) or in both in-phase (I) and quadrature (Q) components of the carrier [1], [16]. In the case of the digital communication systems, these methods correspond to three modulation formats: amplitude-shift keying (ASK), phase-shift keying (PSK), and frequency-shift keying (FSK) [1]. The increased performance, speed, and reliability, and the reduced size and cost of integrated circuits permit to use DSP for the information recovery from the baseband signal [5]. Typically, the M-ary PSK modulation is used in SE high-speed CO-OFDM systems such as quaternary PSK (QPSK) (M=4), 8-PSK (M=8), as well as quadrature amplitude modulation (QAM) such as 4-QAM, 16-QAM, 64-QAM in single or dual polarization [4], [5]. The digital coherent receiver linearly detects incoming signal including phase and polarization diversities and converts this information to digital data by using ADCs while the digital information is processed by DSP circuits [5].

3. High-speed and high SE CO-OFDM system

In this section we present a brief review of the operation principle and architecture of CO-OFDM system. Detailed analysis of CO-OFDM in optical communication systems may be found in the book [4].

A generic optical OFDM system consists of five functional blocks: the RF OFDM transmitter, the RTO up-converter, the optical channel, the OTR down-converter, and the RF OFDM receiver [3], [4]. In such a system the following chain of events occurs [3]. The input data bits

are mapped onto corresponding information symbols of the subcarriers within one OFDM symbol. The digital time domain signal is obtained by using IDFT. It is inserted with the GI Δ_G in order to prevent ISI caused by channel dispersion and converted into the real time waveform through DAC [3]. The baseband signal is up-converted to an appropriate RF band with an IQ mixer/modulator. A linear RTO up-conversion can be achieved by using Mach-Zehnder modulator (MZM) [3]. MZM is mainly used for the bit rates of 40GB/s and higher due to its high modulation performance and the possibility of independent modulation of the electric field intensity and phase [6]. At the receiver, the OFDM signal is down-converted to baseband with an IQ demodulator, sampled by an ADC and demodulated by DFT and baseband DSP to recover the data [3]. A linear OTR down-conversion is provided by a coherent detection described in section 2. The high performance of the CO-OFDM transmission systems has been shown both theoretically and experimentally [8], [17]. A single-channel 1Tb/s CO-OFDM signal consisting of 4104 spectrally-overlapped subcarriers with SE of 3.3bit/s/Hz has been generated, transmitted over 600km standard single mode fiber (SSMF) without amplification and dispersion compensation, and successfully received [17]. However, CO-OFDM system is extremely sensitive to nonlinearity and channel dispersion. The dispersion mitigation with the dispersion compensation fiber (DCF) results in the additional noise and nonlinear effects decreasing the system performance [8].

Consider now the analytical expressions describing the CO-OFDM signals. The MCM transmitted signal $s(t)$ is given by [3]

$$s(t) = \sum_{i=-\infty}^{\infty} \sum_{k=1}^{N_{SC}} c_{ki} s_k(t - iT_s) \tag{7}$$

$$s_k(t) = \Pi(t)\exp(j2\pi f_k t); \Pi(t) = \begin{cases} 1, & 0 < t \leq T_s \\ 0, & t \leq 0, t > T_s \end{cases} \tag{8}$$

where c_{ki} is the i th information symbol at the k th subcarrier, s_k, f_k are the waveform and the frequency of the k th subcarrier, respectively, N_{SC} is the number of subcarriers, and T_s is the symbol period. The optimum detector for each subcarrier could use a filter matched to the subcarrier waveform, or a correlator matched to subcarrier [3]. Eq. (7) shows that the modulation can be performed by IDFT of the input information signal c_{ki}.

The detected information signal c'_{ik} at the output of the correlator has the form [3].

$$c'_{ik} = \int_0^{T_s} r(t - iT_s)\exp(-j2\pi f_k t)dt \tag{9}$$

where $r(t - iT_s)$ is the received time-domain signal. Eq. (9) shows that the demodulation is provided by DFT of the sampled received signal $r(t)$ [3]. The classical MCM uses non-overlapped band-limited signals. In order to prevent overlapping of the band-limited signals, a bank of a large number of oscillators and filters is necessary at the transmitter and the receiver [3]. The cost-efficient design of the filters and oscillators requires that the

channel spacing should be multiple of the symbol rate. As a result, SE reduces and the required bandwidth increases [3].

The OFDM technique permits to use the overlapped signals under the condition that they are orthogonal [7]. The orthogonality condition for any two subcarriers $s_k(t)$ and $s_l(t)$ is given by [3].

$$\frac{1}{T_s}\int_0^{T_s} s_k(t)s_l^*(t)dt = \delta_{kl} = \begin{cases} 1, & k=l \\ 0, & k \neq l \end{cases} \tag{10}$$

Substituting expression (8) into condition (10) we obtain.

$$\exp\left[j\pi(f_k - f_l)T_s\right]\frac{\sin\left[\pi(f_k - f_l)T_s\right]}{\pi(f_k - f_l)T_s} = \delta_{kl} \tag{11}$$

The left-hand side of (11) vanishes when

$$f_k - f_l = \frac{m}{T_s}; m = 1,2,... \tag{12}$$

Then, the two subcarriers $s_k(t)$ and $s_l(t)$ are orthogonal and can be recovered with the matched filters according to (9) without ICI despite the signal spectral overlapping [3].

In the high speed CO-OFDM systems the problem of ISI and ICI caused by the channel dispersion is critical. ISI is caused by the interference between "slow" and "fast" subcarriers. ICI is due to the breaking of the orthogonality condition (12) for the subcarriers [3]. In order to prevent ISI and ICI, CP was proposed that is realized by cyclic extension of the OFDM waveform into GI [3]. The waveform in GI is essentially an identical copy of that in the DFT window [3]. The condition for ISI-free OFDM transmission requires that the dispersive channel time delay spread $t_d < \Delta_G$ [3].

SE is defined as the ratio of net per-channel information data rate B to WDM channel spacing Δf and measured in b/s/Hz [1], [18]. SE of CO-OFDM η is given by [3]

$$\eta = 2\frac{R_s}{B_{OFDM}} \tag{13}$$

where $R_s = N_{SC}/T_s$ is the total symbol rate, $B_{OFDM} = (2/T_s) + (N_{SC} - 1)/t_s$ is the OFDM bandwidth, t_s is the observation period, and the factor of 2 is taking into account two polarizations of the optical fiber modes. Typically, the subcarriers number is large: $N_{SC} \gg 1$. Then eq. (13) takes the form: $\eta \approx 2t_s/T_s$. The optical SE of 3.6bit/Hz can be achieved for QPSK modulation of subcarriers, and can be improved by using higher-order QAM modulation format [3]. However, the addition of CP requires an increase of a bandwidth B_{OFDM} and sampling rate of ADC and DAC. The need for CP can be avoided if WPT is used in CO-OFDM systems instead of DFT and IDFT [13]. This approach will be discussed in the next section.

4. WPT based CO-OFDM

WPT can be used in CO-OFDM instead of the IDFT/DFT since it improves the system performance, and in particular, mitigates the channel chromatic dispersion without CP [13]. In this section we briefly discuss the main features of WPT and its applications to CO-OFDM. The theory and applications of continuous wavelet transform (CWT) and discrete WT (DWT) can be found in a large number of books and articles (see, for example, [13], [14], [19]-[22] and references therein).

CWT $W_T(a,\tau)$ of a given function f(t) with respect to a mother wavelet (MW) $\psi(t)$ is defined as follows [19], [20]

$$W_T(a,\tau) = \frac{1}{\sqrt{|a|}} \int_{-\infty}^{\infty} \psi^*\left(\frac{t-\tau}{a}\right) f(t)dt \qquad (14)$$

where the real numbers a and τ are the scaling and shifting, or translation parameters, respectively, and asterisk means complex conjugation. Note that in many practically important cases MW $\psi(t)$ is real. The functions $\psi^{a,\tau}(s) = |a|^{-1/2}\psi((s-\tau)/a)$ are called wavelets [20]. The set of wavelets is orthogonal and can be used as a basis instead of sinusoidal functions [13]. It is possible to localize the events described by f(t) in time and frequency domains simultaneously by means of WT choosing the appropriate values of the parameters a and τ [19]. For this reason, wavelets are used in the multiresolution analysis (MRA) which decomposes a signal at different scales, or resolutions, using a basis whose elements are localized both in time and in frequency domains [14].

DWT is given by [19], [20]

$$W_T^{m,n}(a,\tau) = a_0^{-m/2} \int_{-\infty}^{\infty} \psi^*\left(a_0^{-m}t - n\tau_0\right) f(t)dt \qquad (15)$$

where m,n∈Z, Z is the set of all integers, and the constants $a_0 > 1, \tau_0 > 1$. Comparison of eqs. (14) and (15) shows that $a = a_0^m$ and $\tau = n\tau_0 a_0^m$ [20]. The orthogonal wavelet series expansions can be successfully used in DSP and multiplexing when the scaling and translation parameters are discrete [14]. In such a case, a signal s(t) ∈V$_0$ can be represented by a smooth approximation at resolution 2^M, obtained by combining translated versions of the basic scaling function $\phi(t)$, and M details at the dyadic scales $a = 2^l, (l = 1, 2, ..., M-1)$ obtained by combining shifted and dilated versions of the MW $\psi(t)$ as follows [14].

$$s(t) = \sum_k 2^{-M/2} c_M[k] \phi\left(2^{-M}t - k\Delta\tau\right) + \sum_{l=1}^{M} \sum_k 2^{-l/2} d_l[k] \psi\left(2^{-l}t - k\Delta\tau\right) \qquad (16)$$

Here a subspace V$_0$∈L²(R), L²(R) is a the linear vector space of square integrable functions, $2^{-l/2}\phi\left(2^{-l}t - k\Delta\tau\right)$ and $2^{-l/2}\psi\left(2^{-l}t - k\Delta\tau\right)$ are the orthonormal bases for the subspaces

$V_l \in L^2(R)$ and $W_l \in L^2(R)$, respectively, $V_l \perp W_l$, (l,k)∈Z, $c_l[k]$ and $d_l[k]$ are the scaling and detail coefficients, respectively, at resolution 2^l, $\Delta\tau$ is the time interval coinciding with the inverse of the free spectral range (FSR). The scaling function $\phi(t)$ and wavelet function ψ(t) satisfy the dilation equations [14], [19], [21]

$$\phi(t) = \sqrt{2}\sum_k h[k]\phi(2t - k\Delta\tau); \psi(t) = \sqrt{2}\sum_k g[k]\phi(2t - k\Delta\tau) \tag{17}$$

where h[k] and g[k] are the coefficients of two half-band (HB) quadrature mirror filters (QMFs) described by the following functions H(ω) and G(ω)

$$H(\omega) = \frac{1}{\sqrt{2}}\sum_k h[k]\exp(-j\omega k\Delta\tau); G(\omega) = \frac{1}{\sqrt{2}}\sum_k g[k]\exp(-j\omega k\Delta\tau) \tag{18}$$

and $\Delta\tau$ is the inverse of their FSR. The functions H(ω) and G(ω) (18) satisfy the conditions [14], [22].

$$\left|H(\omega)\right|^2 + \left|G(\omega)\right|^2 = 1; G(\omega) = \exp(-j\omega k\Delta\tau)H^*\left(\omega + \frac{\pi}{\Delta\tau}\right) \tag{19}$$

The evaluation of the discrete wavelet coefficients is equivalent to filtering the signal s(t) by a cascade of mutually orthogonal bandpass filters [21]. An optical HB filter can be realized by using Mach-Zehnder interferometers (MZIs) [14], [22].

The DWT decomposition procedure is described by the following recursive expressions for the scaling and detail coefficients $c_l[n], d_l[n]$ [14], [22]

$$c_l[n] = \sum_k c_{l-1}[k]h[2n-k]; d_l[n] = \sum_k c_{l-1}[k]g[2n-k] \tag{20}$$

where

$$c_0 = \int s(t)\phi(t - n\Delta\tau)dt \tag{21}$$

In the DWT case only the scaling coefficients $c_l[n]$ are recursively filtered, while the detail coefficients $d_l[n]$ are not reanalyzed [14]. In the case of the WP decomposition both the scaling coefficients $c_l[n]$ and the detail coefficients $d_l[n]$ are recursively decomposed following the same filtering and subsampling scheme, and consequently, all outputs have the same number of samples span over the same frequency bandwidth [14]. The WP decomposition based on the wavelet atom functions $w_{l,m}(t)$ is performed as follows [14]

$$w_{l+1,2m}(t) = \sum_k h[k]w_{l,m}\left(t - 2^l k\Delta\tau\right) \tag{22}$$

$$w_{l+1,2m+1}(t) = \sum_k g[k]w_{l,m}\left(t - 2^l k\Delta\tau\right) \tag{23}$$

where l is the decomposition level, $0 \leq m \leq 2^l - 1$ is the wavelet atom position in the tree, $w_{0,0} = \phi(t)$ and

$$w_{l,m}(t) = \sum_k f_{l,m}[k] \phi(t - k\Delta\tau) \tag{24}$$

and $f_{l,m}[k]$ is the equivalent filter from the root to the (l,m) th terminal recursively evaluated using eqs. (22), (23). The orthogonality condition for WP atoms has the form [14]

$$\int w_{l,m}(t - 2^l n\tau) w_{\lambda,\mu}(t - 2^\lambda k\tau) dt = \delta(l - \lambda)\delta(m - \mu)\delta(n - k) \tag{25}$$

where $(l,\lambda) \in Z$, $0 \leq m \leq 2^l - 1, 0 \leq \mu \leq 2^\lambda - 1$, $(n,k) \in Z$. The waveform orthogonality is used in WPT based OFDM in order to transmit multiple message signals overlapping in time and frequency domains [14]. The time and frequency localization of wavelets can mitigate the optical channel chromatic dispersion which affects only the detail coefficients, or the highpass-filtered versions of the original signal. Then, a selective reconstruction of the wavelet coefficients is necessary [14].

WPTs can provide orthogonality between OFDM subcarriers similarly to DFT, and consequently, DWPT can replace DFT in the CO-OFDM system [13]. The all-optical WPT based CO-OFDM (WPDM) system has been proposed where the digital sequences are encoded by a set of orthogonal waveforms [13], [14]. The system performance is improved due to the orthogonal properties (25) of the wavelet atoms (22)–(24) and their overlapping in time and frequency [13], [14]. Each optical pulse is transformed into the corresponding wavelet atom function at the device output under the conditions that the input bit duration $t_{bit} = \Delta\tau$ and the processing gain $F = 2^l$ is equal to the number of simultaneous users [14]. In the WPT-OFDM system each channel occupies a WP [13]. At the transmitter, IDWPT reconstructs the time domain signal from WPs; at the receiver DWPT is used in order to decompose the time domain signal into different WPs by using successive low-pass and high-pass filtering [13]. Unlike IDFT/DFT system, in the IDWPT/DWPT OFDM system the basis function wavelets are finite in time, the inter-symbol orthogonality in WT is maintained due to the shift orthogonal property of waveforms, and symbols are overlapped in time domain [13]. As a result, the symbol duration increases, providing the tolerance with respect to the chromatic dispersion and eliminating the need of CP [13].

Consider the computational complexity C_{WPT} of WPT-OFDM defined as the total required number of complex multiplications [23]. It depends on the specific type of wavelets and system configuration. The complexity of one basic block C_{BB} determined by the convolution between complex input data and real QMFs, and the total complexity C_{WPT} are given by, respectively [23]

$$C_{BB} = L_{QMF}; C_{WPT} = (N - 1) L_{QMF} \tag{26}$$

where L_{QMF} is QMF length, N is the number of subcarriers. WTP-OFDM reduces the complexity by a factor of 6 to 10 for different wavelets in the range of moderate accumulated dispersion as compared to FFT based CO-OFDM without CP [23].

The performance of a digital optical communication systems is characterized by the bit error rate (BER) defined as the average probability of incorrect bit identification [1]. The simulations of the BER for WPT-OFDM and FFT based OFDM have been carried out using different wavelets, optical SNR of 20dB , chromatic dispersion parameter of 17ps/(nm·km), and forward error correction code (FEC) threshold of 10^{-3} [13]. The results show the chromatic dispersion tolerance of 5600 ps/nm and the longest distance of 330km for SSMF for the Johnston64 (E) wavelet [13].

We have carried out the numerical simulations of BER dependence on the transmission distance in the single polarization regime for the WPT-OFDM system without CP, with GI length of 5% of the symbol interval, and for generic IDFT/DFT systems with values of CP length from 5% up to 30% of the symbol interval. We used the single-polarization signal with the optical carrier frequency $f_{opt} = 193.1THz$, with 128 subcarriers. An optical fiber is characterized by the attenuation of 0.2dB/km and chromatic dispersion parameter of 17ps/(nm·km). We assumed that the efficient transmission can be realized with the BER less than the FEC threshold of $2\cdot10^{-2}$. PMD has not been taken into account. At the receiver, we used window synchronization Schmidl - Cox algorithm and 1 tap equalizer in frequency domain.

The BER dependence on the distance for the Haar WPT-OFDM and FFT CO-OFDM with different CPs is shown in Figure 2.
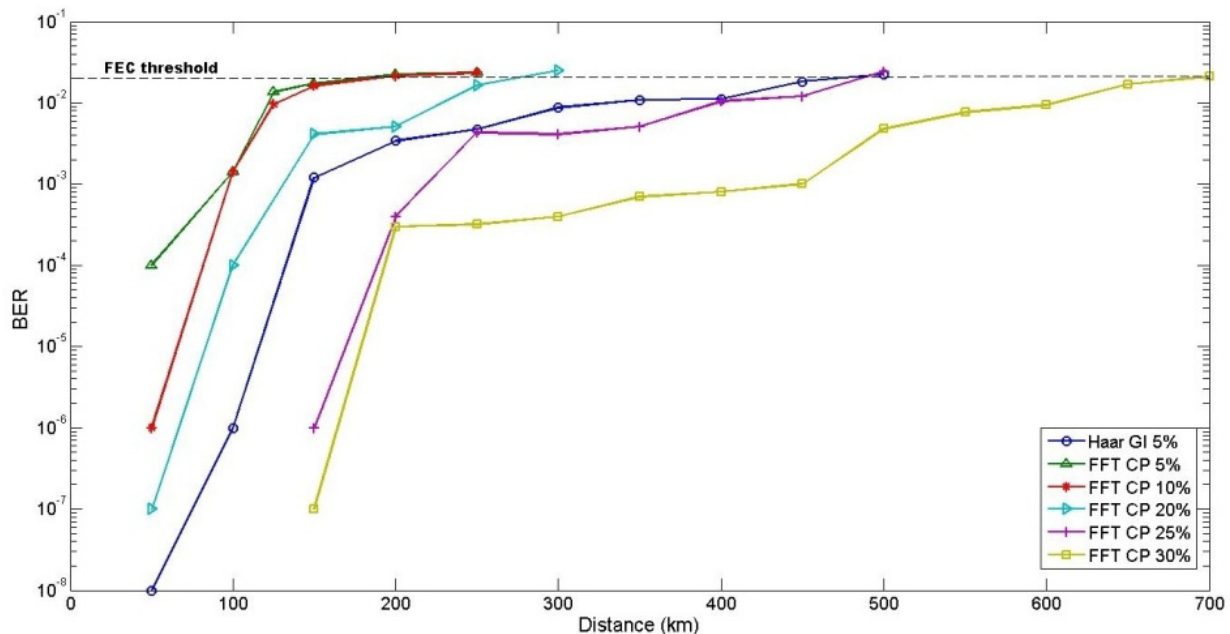

Figure 2. BER dependence on the transmission distance for FFT CO-OFDM with different CPs and WPT-OFDM without CP, with GI 5%

The results clearly show that WPT-OFDM provides the efficient transmission up to 500km without CP with 5% GI, while the FFT based CO-OFDM may achieve the same distance with the CP length of 25% of the symbol interval which substantially reduces SE of the communication system.

5. Passive Si-photonic components for all-optical signal processing

In this section we discuss the implementation of passive WPT-OFDM system components based on the Si photonics and a novel hierarchical architecture of the 1Tb/s WPT-OFDM transmission system that can be realized by using these components.

5.1. SOI optical components

The practical implementation of all-optical signal processing would require some extent of device integration. Much effort is dedicated over the last two decades to the development of photonic integrated circuits (PICs), which bring together multiple discrete devices on a single substrate. Integration helps to minimize the losses associated with the coupling of light in and out of devices, to enhance functionality, and to reduce cost and footprint. Numerous material platforms are prevalent in PICs, such as $LiNbO_3$, GaAs, InP and SiO_2. Among those platforms, the SOI wafer structure stands out as an advantageous choice for the realization of passive devices, such as couplers, interferometers, arrayed-waveguide gratings etc [24], [25]. Silicon is a low-cost material with an excellent crystalline quality, high thermal conductivity and high optical damage threshold. It is transparent over a broad range of wavelengths of 1.1-7 μm, including the telecommunication wavelengths. The silica SiO_2 lower cladding of SOI wafers provides a large contrast in refractive index with respect to silicon, which allows for the tight confinement of light into sub-micron structures. The fabrication of photonic devices in SOI can benefit from the advanced manufacturing technology of electronic integrated circuits. Silicon photonic devices may lead to a true merger of optics alongside electronics in unified devices. The realization of modulation of light on the silicon material platform is more challenging. The concentration of free charges in silicon changes the real and imaginary parts of the refractive index, and this effect in pure silicon is more strongly pronounced than the Pockels effect, the Kerr effect and the Franz-Keldysh effect [26]. Most of the fast modulators integrated on Si are based on free-carrier concentration variations [27]. Optical modulation using SiGe/Si and all-silicon phase shifters based on carrier depletion has been investigated theoretically and experimentally [27]. An all-silicon phase-shifter based on carrier depletion in a doped layer inserted into a PIN diode has been demonstrated [28]. SiGe/Si and all-silicon modulators can be integrated in rib waveguides and in MZIs [27]. Another modulation technique for SOI optical devices is based on the thermo-optic effect, in which the refractive index n of silicon is varied by applying heat to the material [24]. The thermo-optic coefficient in silicon is given by $dn/dT = 1.86 \times 10^{-4} K^{-1}$, and the refractive coefficient variation of $\Delta n = 1.1 \times 10^{-3}$ for the controllable temperature increase of 6K [24]. It has been shown experimentally that a 500μm length device thermally isolated from the substrate can provide a phase shift of π radians for an applied power of 10mW [24].

5.2. Example of SOI MZM for all-optical signal processing

In this section we present an example of the SOI based MZI which can realize the WPT operation. The most basic family of wavelet shapes is the Haar transform, proposed initially by Alfred Haar in 1910 [19]. The Haar wavelet and scaling functions $\psi(t), \phi(t)$ and the filter coefficients h[n], g[n] have the form, respectively [13], [19].

$$\psi(t) = \begin{cases} 1, 0 \le t < \dfrac{1}{2} \\ -1, \dfrac{1}{2} \le t < 1; \\ 0, t < 0, t \ge 1 \end{cases} \phi(t) = \begin{cases} 1, & 0 \le t < 1 \\ 0, & t < 0, t \ge 1 \end{cases} \tag{27}$$

$$h[n] = \frac{1}{\sqrt{2}}(-1,1), g[n] = \frac{1}{\sqrt{2}}(1,1) \tag{28}$$

Note that the equivalent definitions $h[n] = (1,1)/\sqrt{2}, g[n] = (1,-1)/\sqrt{2}$ also may be used [21]. Since it is the simplest to implement, we adapt it in the proposed realization of the WPT based CO-OFDM photonic integrated circuit. An n-points signal is decomposed into two groups of n/2 samples. The first group is the sum of pairs of c[n] of the original signal, and can be described as the output of a discrete low-pass filter (LPF) followed by a down-sampling operation by a factor of two. The second group describes the differences between pairs d[n], and can be represented as the output of a discrete high-pass filter (HPF) followed by factor of two down-sampling operation [14]. The Haar WPT can be described by the scheme shown in Figure 3. Here s[n] is the input signal, g[n] and h[n] are the discrete HPF and LPF impulse responses.
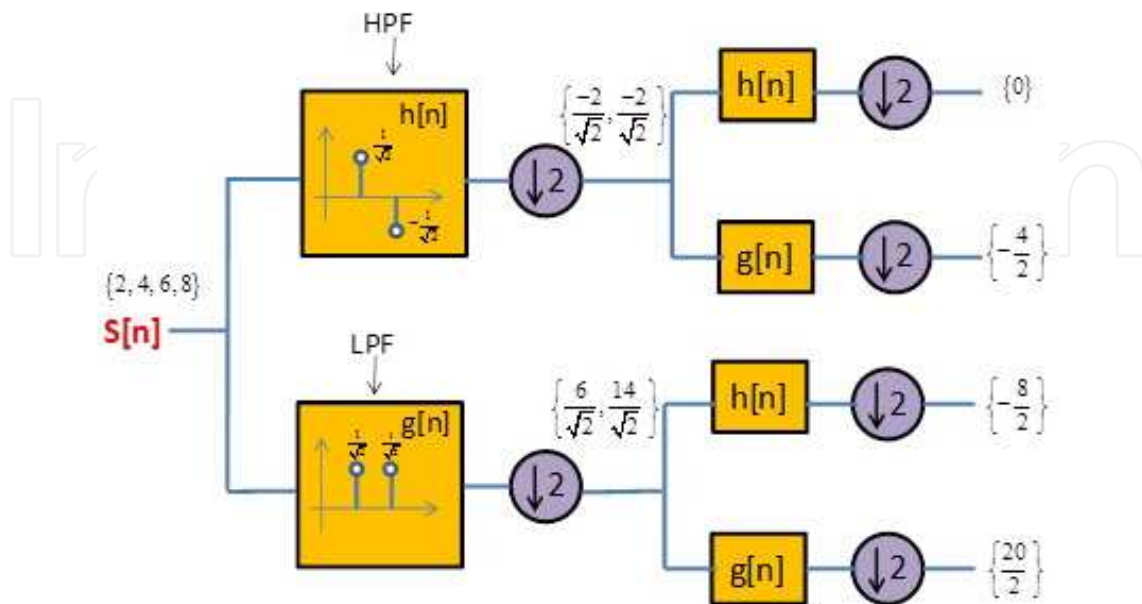

Figure 3. Two levels Haar wavelet-packet decomposition (WPD)

The inverse operation recovers the original signal from its decomposition coefficients. Its scheme is shown in Figure 4. Here S[n] is the output signal, g[n] and h[n] are the discrete HPF and LPF impulse responses, c[n] and d[n] are the approximation and detail coefficients respectively mentioned above.
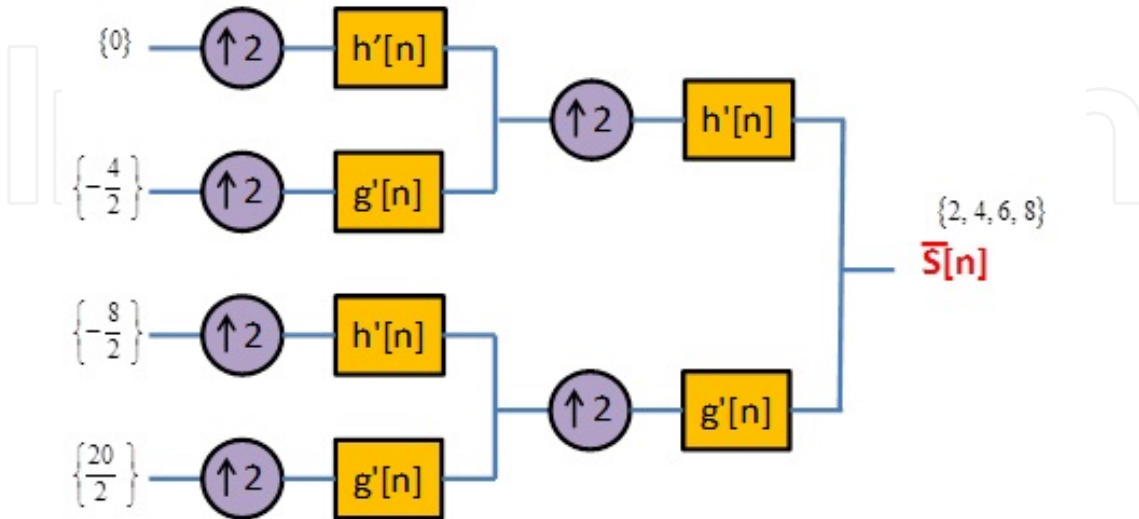

Figure 4. Haar inverse wavelet-packet decomposition (IWPD) transform

The realization of Haar wavelet packet decomposition (WPD) transform and the corresponding inverse wavelet packet decomposition (IWPD) in an optical integrated circuit was theoretically suggested by Gabriella Cincotti and co-workers [14], [22], [29], [30]. The method is based on the following MZI delay line architecture shown in Figure 5.

(a) Haar -IWPD   (b) Haar -WPD
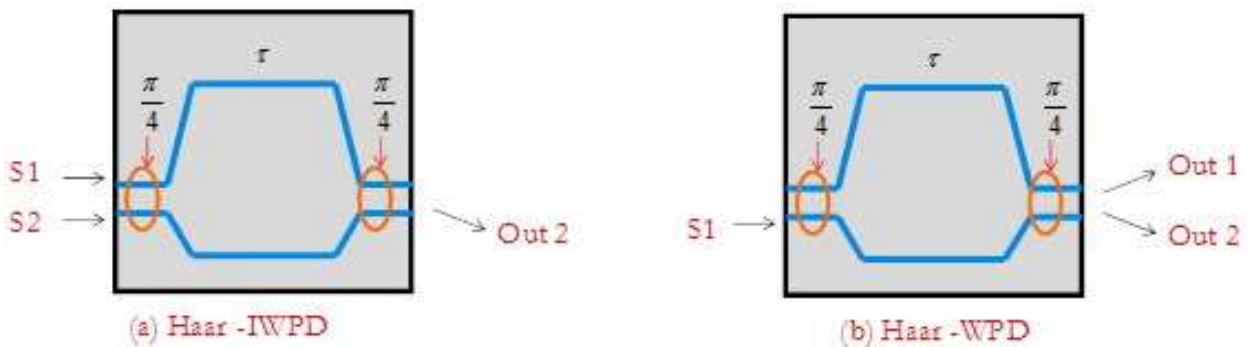
Figure 5. Optical implementation of Haar WPD / IWPD based on MZI. Left: Haar-IWPD used for the transmitter unit. Right: Haar-WPD used for the receiver unit.

The IWPD is represented by the optical field $E_{out2}(t)$ at the lower output of a MZI that is driven by two inputs $S_{1,2}(t)$.

$$E_{out2}(t) = \frac{1}{2}\left[-jS_1(t) + S_2(t)\right] + \frac{1}{2}\left[-jS_1(t-\tau) - S_2(t-\tau)\right] \tag{29}$$

Expression (29) shows that a single MZI could provide the sum and the difference of its two input fields, in series, in one of its output ports. The operation is equivalent to the LPF and

HPF operation of the inverse Haar IWPD. Similarly, the same MZI can generate the sum of successive values in one of its input ports at one output $E_{out2}(t)$, and the difference of the same values at the other output $E_{out1}(t)$, in parallel.

$$E_{out1}(t) = \frac{1}{2}\left[S_1(t) - S_1(t-\tau)\right]; E_{out2}(t) = -j\frac{1}{2}\left[S_1(t) + S_1(t-\tau)\right] \tag{30}$$

The latter configuration described by expression (30) can realize the Haar WPD. Hence, MZIs can function as a basic building block of a discrete Haar WPD and IWPD. As can be seen in equations (29) and (30), the MZI realization of the WPD includes an additional relative phase shift of 90° in between the two inputs/outputs, which is not part of the Haar formalism. This additional phase must be compensated for. Furthermore, the optical path lengths connecting between cascaded MZIs cannot be controlled at the fabrication stage to a sub-wavelength precision. Hence, metallic resistors must be deposited in proximity to the waveguides [31], [32]. The driving of currents through the resistors would locally heat the nearby silicon structure, and modify its refractive index through the thermo-optic effect mentioned above [24]. A schematic drawing of a single MZI with the thermo-optic phase-shifters is shown in Figure 6.
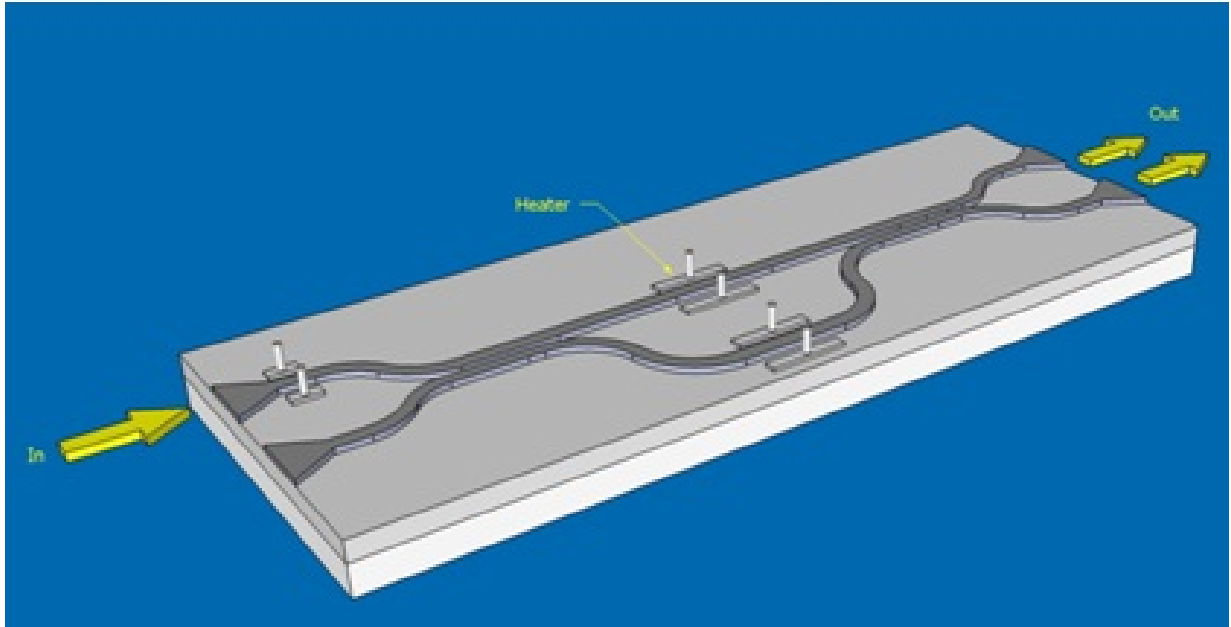

Figure 6. A schematic drawing of a single MZI stage used in a Haar WPD receiver including three thermo-optic phase-shifters

Three-stage MZI-based photonic integrated circuits for the realization of Haar WPT-OFDM encoding and decoding based on the single MZI stage are shown in Figures 7, 8.

In the Haar WPT-OFDM encoder presented in Figure 7, S_1-S_8 are low rate input data channels, with a seven-bits zero padding. The output is the multiplexed Haar transform signal.
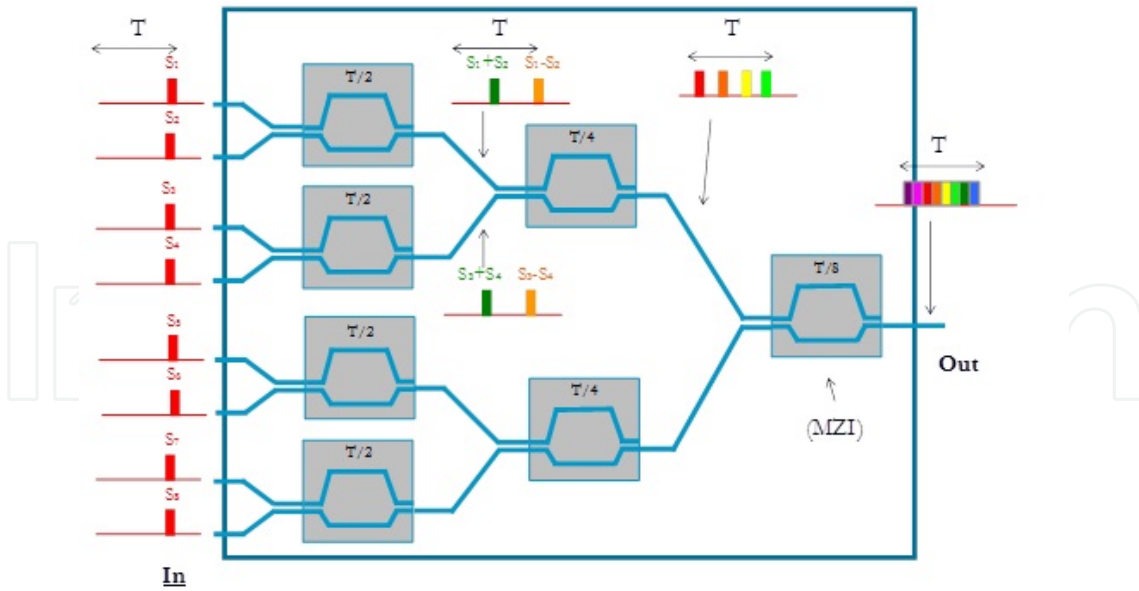
Figure 7. All-optical Haar WP Encoder used as optical transmitter

In the all-optical Haar WP Decoder shown in Figure 8, the input signal is constructed from eight data channels, which are recovered individually at the eight outputs. The output channels must be down sampled by factor of 8.
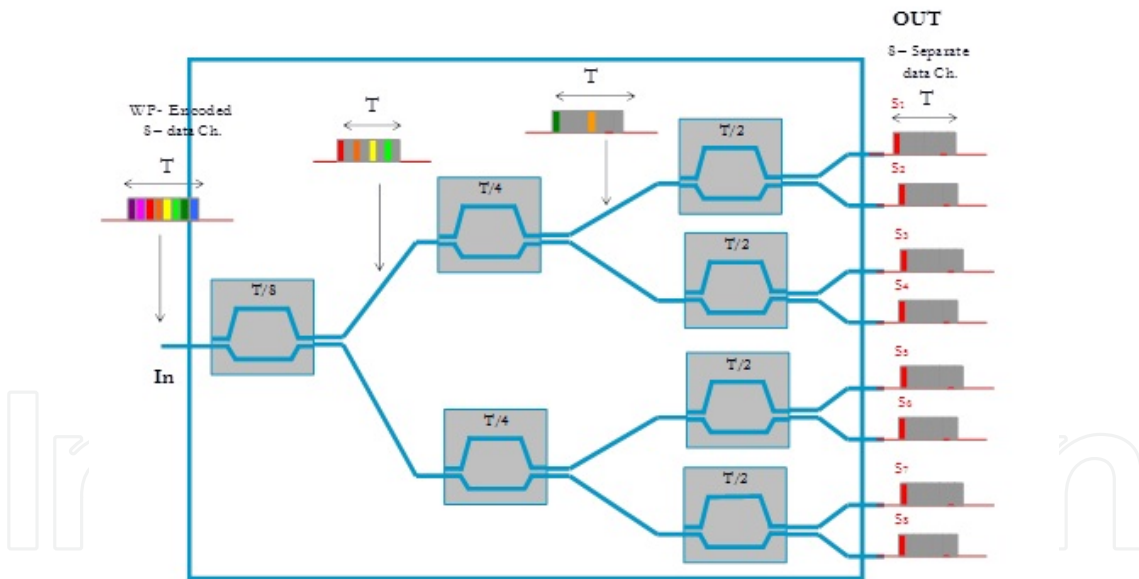

Figure 8. All-optical Haar WP Decoder used as an optical receiver

The all-optical WP encoder calculates the Haar IWPD of eight coefficients, incoming from eight parallel input values. The reconstructed signal appears in series at the output of the circuit. Note that padding by seven zeros is necessary between successive bits at each input, so that the transform coefficients of one input parallel word do not overrun those of the next word at the output [9], [33], [34]. The zero padding is the optical-domain equivalent of the up-sampling that is part of a digital IWPD. Similarly, a proper gating is necessary at the each of the eight outputs of the decoder circuit, since the original data is only reconstructed

at specific time slots within the symbol duration [33]. The remainder of the symbol duration is occupied by noise-like ISI.

A WPT based CO-OFDM communication network, employing the encoding and decoding PICs, is shown in Figure 9. Light from a CW laser diode is split in eight paths. Light in each path is individually modulated by a separate stream of data, which are prepared with the necessary zero padding as described above. The eight channels are multiplexed by the WPT-OFDM PIC. At the other end of the link, each of the eight outputs of the WPT-OFDM decoder PIC is separately gated by an electro-optic switch and detected.

The SOI waveguide is a basic component of the Si photonic systems. We calculated the modal profile of such a waveguide in a single mode regime for each polarization of the optical wave. The SOI waveguide cross-section and the modal profile are shown in Figure 10. The analysis of such waveguides can be carried out only by numerical methods [35]. We used the commercial software modeling (COMSOL). The modal field distribution (Figure 10b) clearly shows the electric field confinement in the waveguide core.

A basic building block of a MZI is a directional coupler. Couplers are realized by bringing two SOI waveguides in close proximity for a certain length Z_0. The degrees of freedom in the design are the length and gap between the SOI waveguide cores. A relatively large gap of the order of magnitude of 300nm is advantageous with respect to fabrication imperfections. COMSOL simulations were used to calculate the coupling coefficient κ_{ab} between two waveguides separated by a chosen gap. An even splitting ratio of incoming optical power between the two outputs is obtained when the two waveguides remain in proximity over a length $L = \pi / (4\kappa_{ab})$. The simulation results are shown in Figure 11.
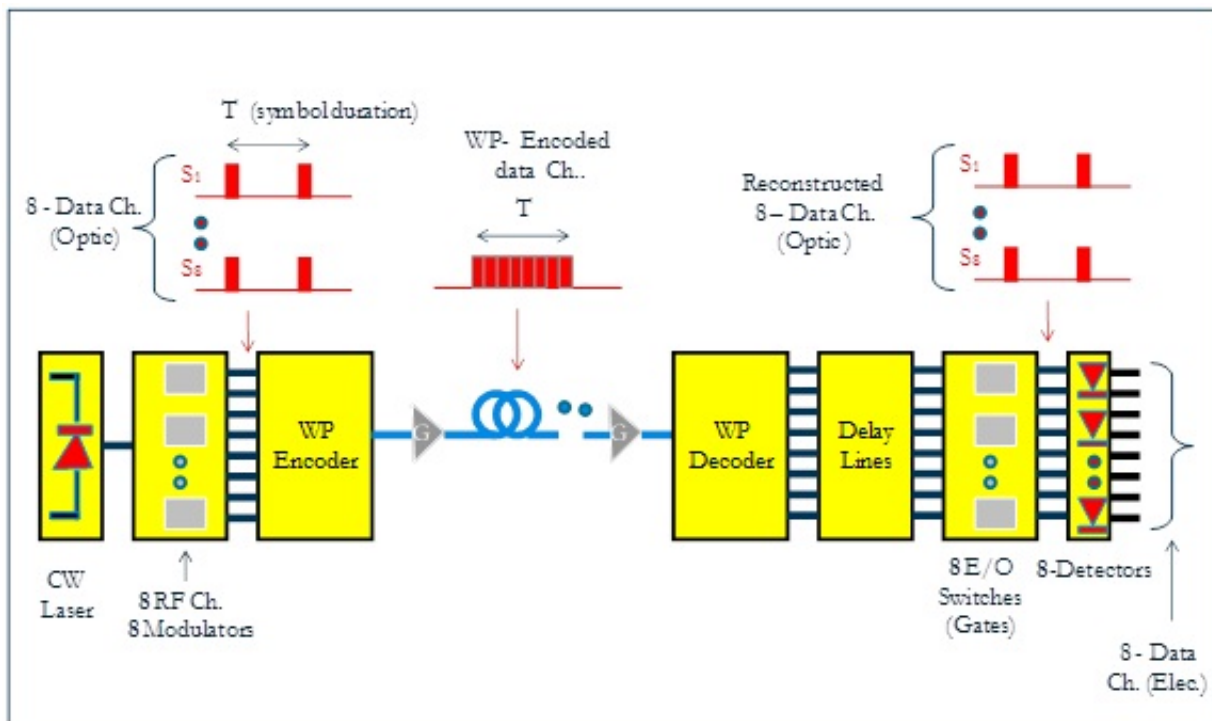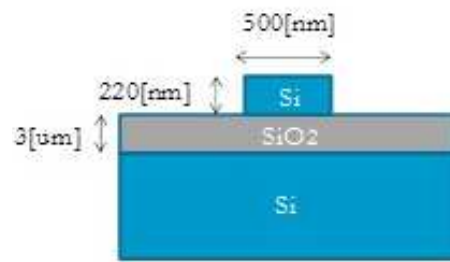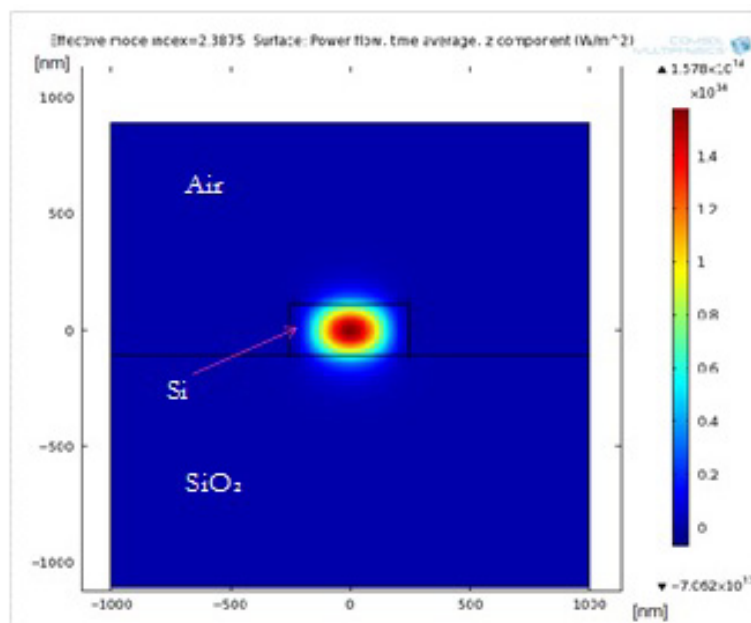

Figure 9. WPT based CO-OFDM data channel based on transmitter and receiver PICs

(a)

(b)

Figure 10. A single mode SOI-based waveguide; (a) schematic diagram; (b) COMSOL simulation of the transverse profile for the EM mode field super-imposed on the waveguide cross section

Consider now the differential delays of the MZIs. As discussed earlier, different stages in the cascaded MZI PIC require different delays. The basic delay unit is T/8, where T is the symbol duration. For a data rate of 2.5 GSymbols/s for each of the eight multiplexed channels, the fundamental delay unit is 50psec, which corresponds to a physical length of about 3.5mm in SOI waveguides. The heat dissipation from aluminium heaters in proximity of the SOI waveguides was simulated, once more using COMSOL. Figure 12 shows the resulting temperature profile. The Al heaters are heated by an external current up to 60°C. Simulation results show that a temperature in the Si core of the SOI waveguide is 40°C compared to 20°C in the unheated regions. This temperature difference stems from the attachment of the back end of the PIC to a 20°C heat sink.
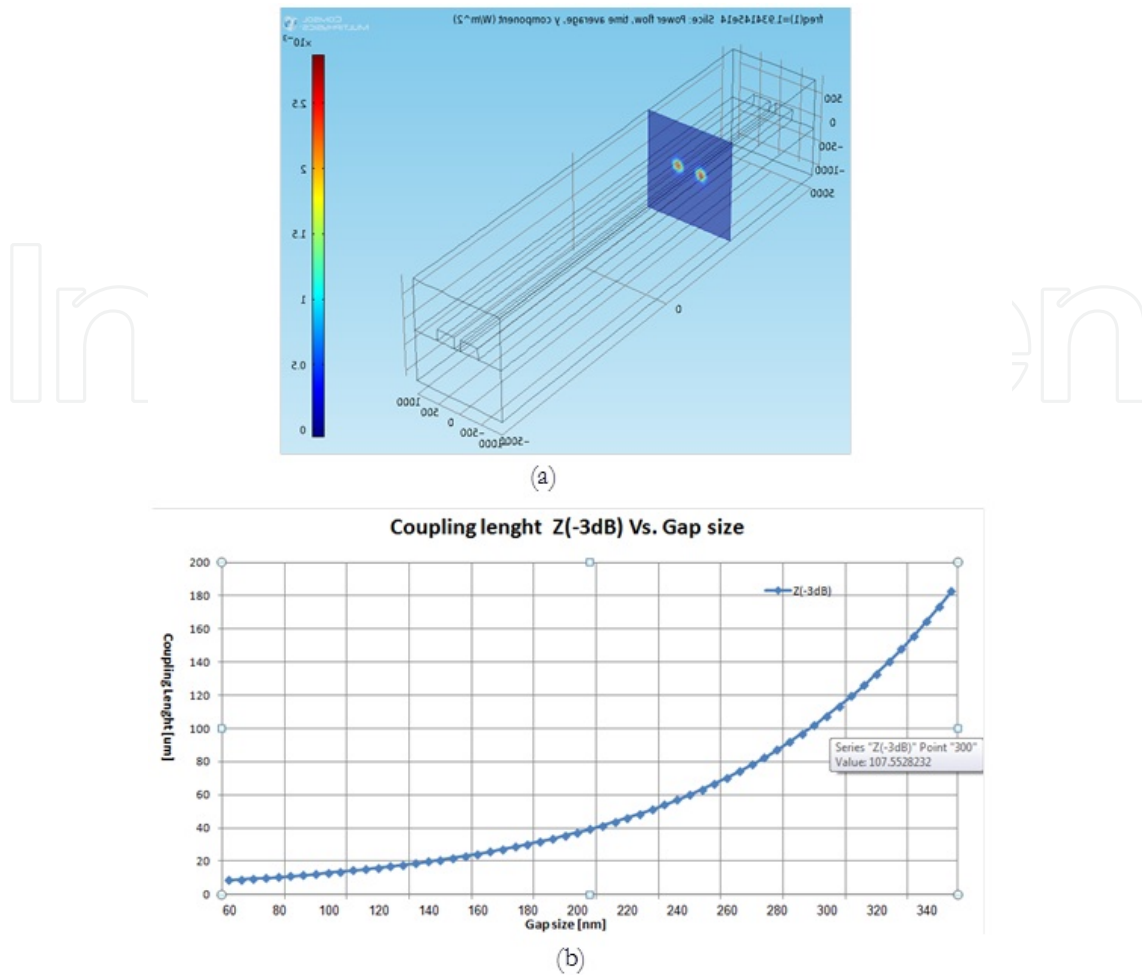
(a)

(b)

Figure 11. Coupler dimensions design with COMSOL software simulations: (a) an example of a three-dimensional modelling of a directional coupler; (b) calculated coupling length that is required between two parallel waveguides as a function of the gap size. The coupling length for the chosen gap size of 300 nm is approximately 110μm
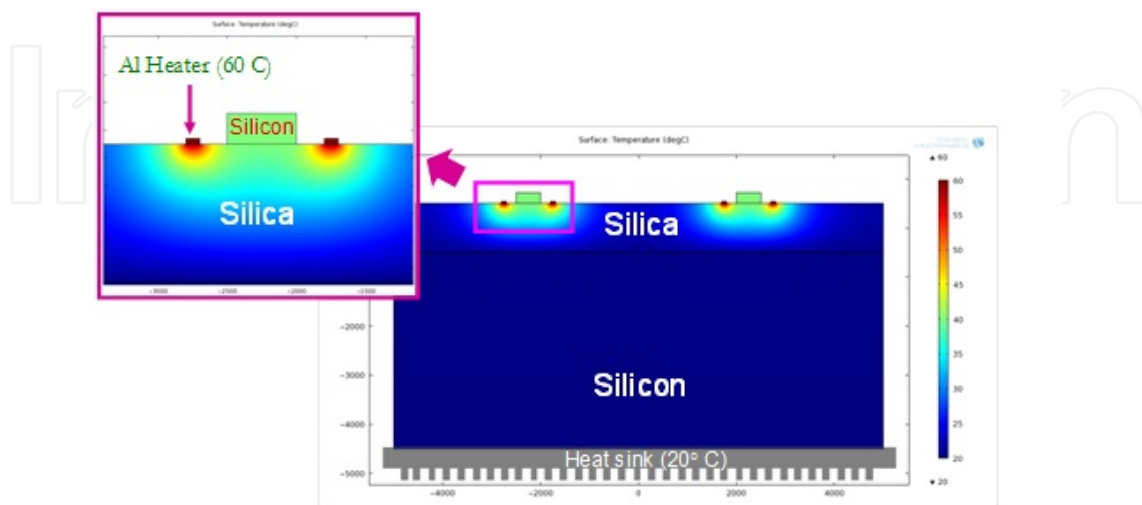

Figure 12. Cross section of heat dissipation in an SOI waveguide with the aluminium heaters located in both sides of the SOI waveguide

5.3. Hierarchical architecture and performance of the WPT based OFDM system

The DSP in CO-OFDM systems is carried out by the algorithms realized with the field programmable gate array (FPGA) and application specific integrated circuit (ASIC) electronic processors. Their computational power is limited with the operation rate of the VLSI electronic elements. For this reason, the electronic "bottleneck" can be eliminated and the system operation rate can be improved if high data rates signal processing is realized by all-optical methods such as all-optical WPT-OFDM.

We proposed a novel hierarchical architecture of the 1Tb/s transmission system based on WPT-OFDM in order to reduce the computational complexity of the DSP algorithms [15]. The hierarchical architecture concept is based on the separation of low bit rate and high bit rate signal channels, unlike the system discussed in Ref. [13]. We used an IDWPT/DWPT system based on the Haar WPT with the wavelet function $\psi(t)$, scaling function $\phi(t)$, and filter coefficients g[n] and h[n] given by eqs. (27), (28) [13], [19].

The WPT-OFDM hierarchical transmitter and receiver are shown in Figures 13 and 14, respectively.

The high data rate bands are multiplexed using all-optical IDWPT. The transmitter includes IQ modulator. QAM 16, QAM 4 and other multilevel modulation formats can be used for each subband. Subbands are multiplexed in electrical domain also by utilizing the IDWPT. At the receiver side, the multiband signal is demultiplexed into the 8 bands using all-optical
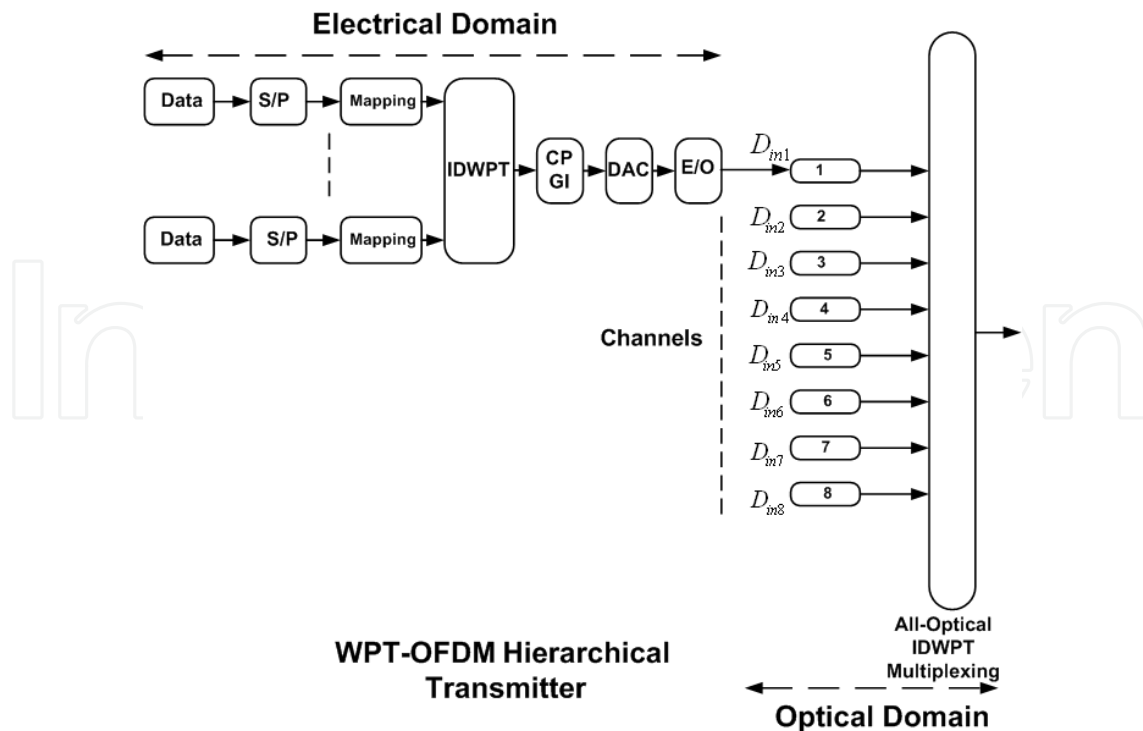

Figure 13. Hierarchical architecture of the WPT-OFDM transmitter (S/P - serial/parallel; E/O - electrical/optical)
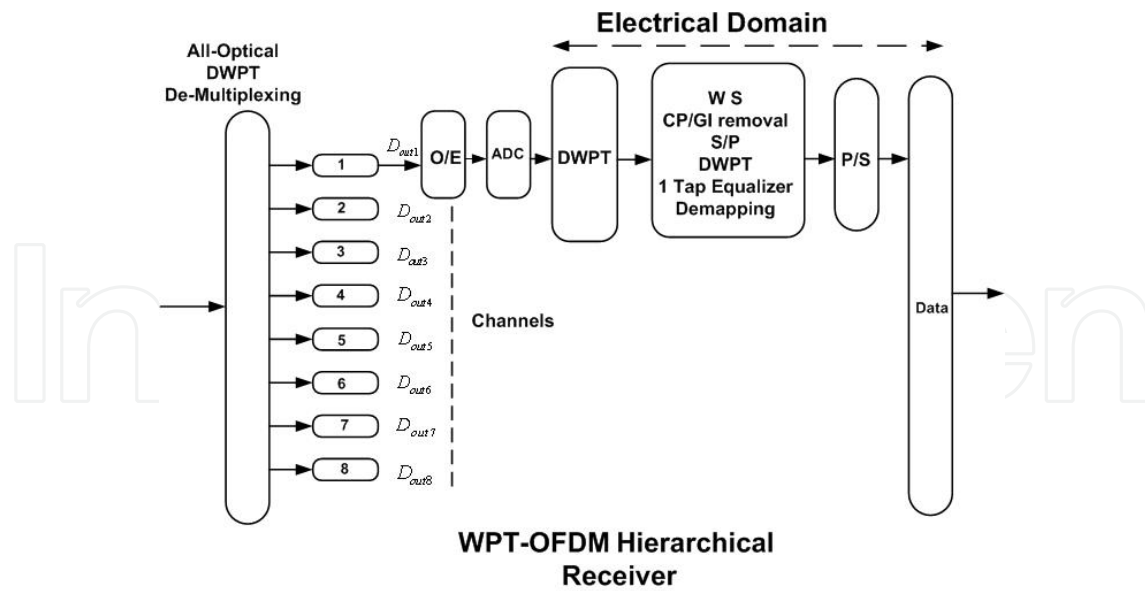
Figure 14. Hierarchical architecture of the WPT-OFDM receiver (O/E - optical/electrical, WS-window synchronization, S/P-serial/parallel, P/S-parallel/serial)

filters and consequently demultiplexed into the subbands in the electrical domain by the DWPT. The performance of the WPT-OFDM communication system based on the hierarchical architecture has been investigated theoretically taking into account the 10% non-ideality of the system devices and the white Gaussian noise model. We used the modulation format QAM 16, 8 level decomposition, the bit rate of 500Gb/s. The 500Gb/s multiple band consists of eight 62.5Gb/s bands. The simulated constellation of the transmitter-receiver "back-to-back" system, i.e. without optical fiber link is shown in Figure 15.
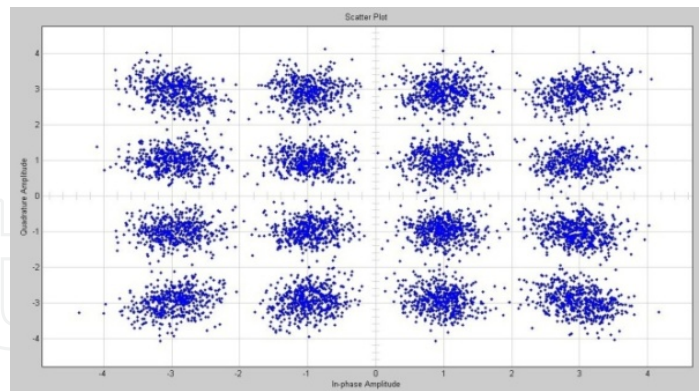

Figure 15. Constellation diagram for all-optical WPT-OFDM with a 500Gb/s bit rate, QAM-16 modulation format and 8 level decomposition

The constellation clearly shows the high performance of the transmitter-receiver system.

6. Conclusions

We discussed in this chapter the structure, operation principle and basic properties of the all-optical high SE CO-OFDM systems. The CO-OFDM is the most promising modulation

method in the modern optical systems combining the advantages of the coherent detection and OFDM modulation. However, the high data rate transmission is strongly influenced by the optical channel chromatic dispersion and PMD. As a result, the transmission system performance significantly deteriorates due to ISI and ICI. The dispersion influence can be mitigated by an appropriately chosen CP. Unfortunately, a long enough CP would decrease the system SE. The problem can be solved and the necessity of CP may be eliminated if a generic DFFT based CO-OFDM is replaced with a WPT-OFDM since WPs are localized both in time and frequency domains. The simulation results show that WPT-OFDM system provides a 500 km transmission distance at the FEC level of 2×10^{-2} without CP, with a small 5% GI. We proposed a novel hierarchical architecture of the WPT-OFDM system based on the separation of the low data rate and high data rate signal processing. The former ones are processed in the electrical domain, while the latter ones undergo the all-optical processing. The numerical simulations show that such an approach improves the WPT-OFDM system performance which is demonstrated by the constellation of a signal with QAM 16 modulation. The WPT-OFDM all-optical signal processing units can be implemented by using the passive SOI waveguide components. The passive components of this architecture are the wavelet filters realized by the SOI waveguide based MZIs. The change of the Si refraction index is realized by using the thermo-optic effect. We presented the numerical simulations of the Haar wavelet filters for all-optical signal processing based on such MZIs. The modal profile of a SOI waveguide in a single mode regime for each polarization of the optical wave has been calculated.

Author details

Y. Ben Ezra
Holon Institute of Technology (HIT), Holon, Israel;
Optiway Integrated Solutions LTD, Rosh Haayin, Israel

B.I. Lembrikov
Holon Institute of Technology (HIT), Holon, Israel

Avi Zadok, Ran Halifa
School of Engineering and Institute for Nano-Technology and Advanced Materials, Bar-Ilan University, Israel

D. Brodeski
Optiway Integrated Solutions LTD, Rosh Haayin, Israel

Acknowledgement

7. References

[1] Agrawal, G.P. Fiber-Optic Communication Systems, Wiley, New York, 2002.

[2] Ran, M; Ben Ezra, Y. and Lembrikov B.I. Ultra-wideband Radio-over-optical-fibre Technologies, In: Kraemer, R. & Katz, M. D. (Eds.) Short-Range Wireless Communications, Chichester, England: Wiley; 2009, p271-327.

[3] Shieh, W.; Bao, H. and Tang, Y. Coherent optical OFDM: theory and design. Optics Express, Vol.16, No. 2, January 2008, 841-859.

[4] Shieh, W. and Djordjevic, Ivan. Orthogonal Frequency Division Multiplexing for Optical Communications, Academic Press, 2010.

[5] Kikuchi, K. Coherent optical communication systems, In: Kaminov, I. P.; Li, T. & Willner, A. E. (Eds.) Optical Fiber Telecommunications VB: Systems and Networks, Amsterdam, London, New York: Academic Press; 2008. p91-129.

[6] Winzer, J. P. and Essiambre, R.-J. Advanced Modulation Formats for High-Capacity Optical Transport Networks, IEEE Journal of Lightwave Technology December 2006; 24(12) 4711-4728.

[7] Armstrong, J. OFDM for Optical Communications, IEEE Journal of Lightwave Technology, February 2009; 27(3) 189-204.

[8] Tang, Y. and Shieh, W. Coherent optical OFDM transmission up to 1 Tb/s per channel. Journal of Linghtwave Technology, August 15, 2009; 27(16) 3511-3517.

[9] Hillerkuss, D.et al. Simple all-optical FFT scheme enabling Tbit/s real-time signal processing, Optics Express, April 2010; 18(9) 9324-9340.

[10] Wang, X.; Ho, P., and Wu, Y. Robust Channel Estimation and ISI Cancellation for OFDM Systems with Suppressed Features, IEEE Journal on Selected Areas in Communications, May, 2005; 23(5) 963-972.

[11] Lai, Hung-Quoc; Siriwongpairat, W. Pam, and Liu, K.J. Ray. Performance Analysis of Multiband OFDM UWB Systems with Imperfect Synchronization and Intersymbol Interference. IEEE Journal of Selected Topics in Signal Processing, October 2007; 1(3) 521-534.

[12] Armstrong, J. Analysis of New and Existing Methods of Reducing Intercarrier Interference Due to Carrier Frequency Offset in OFDM, IEEE Transactions on Communications, March 1999; 47(3) 365-369.

[13] Li, An; Shieh, W. and Tucker, Rodney S. Wavelet packet transform-based OFDM for optical communications, Journal of Linghtwave Technology, December 15, 2010; 28 (24) 3519-3528.

[14] Cincotti, G.; Moreolo, M.S. and Neri, A. Optical Wavelet Signals Processing and Multiplexing, EURASIP Journal on Applied Signal Processing, 2005;10, 1574-1583.

[15] Ben-Ezra, Y.; Brodeski, D.; Zadok, A.; Califa, R.; Lembrikov, B.I. 1Tbps Transmission System Based on Hierarchical Approach to Wavelet Packet Transform OFDM. Proceedings of the 13th International Conference on Transparent Optical Networks (ICTON 2011), Stockholm, Sweden, June 26-30 2011, Tu.A5.2 (1-4).

[16] Ip, Ezra; Lau, A.P.T.; Barros, D.J.F.; Kahn, J.M. Coherent detection in optical fiber systems. Optics Express, January 2008; 16(2) 753-791.

[17] Ma, Yiran; Yang, Qi; Tang, Y.; Chen, Simin & Shieh, W. 1 Tb/s single-channel coherent optical OFDM transmission over 600-km SSMF fiber with subwavelength bandwidth access, Optics Express, May 2009; 17(11) 9421-9427.

[18] Bigo, S. Multiterabit DWDM terrestrial transmission with bandwidth-limiting optical filtering. IEEE Journal of Selected Topics in Quantum Electronics, March/April 2004; 10(2) 329-340.

[19] Rao, R.M.& A.S. Bopardikar, A. S. Wavelet Transforms. Introduction to Theory and Applications. Reading, Massachusetts: Addison-Wesley; 1998.

[20] Daubechies, I Ten Lectures on Wavelets. Philadelphia, Pennsylvania: Society for Industrial and Applied Mathematics; 2006.

[21] Sarkar, K.T.; Salazar-Palma, M.; Wicks, M.C. Wavelet Applications in Engineering Electromagnetics. Boston: Artech House; 2002.

[22] Moreolo, M. S.; Cincotti, G. and Neri A. Synthesis of optical wavelet filters, IEEE Photonics Technology Letters. July 2004, 16 (7) 1679-1681.

[23] Bulakci, Ö.; Schuster, M.; Bunge, C.-A.; Spinkler, B.; Hanik, N. Wavelet Transform Based Optical OFDM. In: Optical Fiber Communication (OFC), collocated National Fiber Optic Engineers Conference, 2009 Conference on (OFC/NFOEC), 2009, pp. 1-3.

[24] Reed, G. T. and Knights, A. P. Silicon photonics. An introduction. Chichester, England: Wiley; 2004.

[25] Reed, G. T., editor. Silicon photonics. The state of the art. Chichester, England: Wiley; 2008.

[26] Reed, G. T.; Mashanovich, G.; Gardes, F.Y, & Thomson, D.J. Silicon optical modulators, Nature Photonics. August 2010; 4, 518-526.

[27] Marris-Morini, D. et al. Recent progress in high-speed silicon-based optical modulators. Proceedings of the IEEE, July 2009; 97(7) 1199-1215.

[28] Marris-Morini, D. et al. Optical modulation by carrier depletion in a silicon PIN diode, Optics Express, October 2006; 14(22) 10838-10843.

[29] G. Cincotti, G. Full optical encoders/decoders for photonic IP routers, Journal of Lightwave Technology, vol. 22, no. 2, (February 2004) 337- 342.

[30] Moreolo, M. S. and Cincotti, G. Compact low-loss planar architectures for all-optical wavelet signal processing, In: Transparent Optical Networks, 2005, Proceedings of 2005 7th International Conference, 2005, vol. 1, pp. 319- 322.

[31] Densmore, A. et al. Compact and low power thermo-optic switch using folded silicon waveguides, Optics Express, June 2009; 17(13) 10457-10465.

[32] Harjanne, M.; Kapulainen, M.; Aalto, T. and Heimala, P. Sub-µs switching time in silicon-on-insulator Mach-Zehnder thermooptic switch. IEEE Photonics Technology Letters, September 2004; 16(9) 2039-2041.

[33] Hillerkuss, D. et al. Single source optical OFDM transmitter and optical FFT receiver demonstrated at line rates of 5.4 and 10.8 Tbit/s, In: Optical Fiber Communication (OFC), collocated National Fiber Optic Engineers Conference, 2010 Conference on (OFC/NFOEC), 2010, pp. 1-3.

[34] Hillerkuss, D. et al. 26 Tbit s-1 line-rate super-channel transmission utilizing all-optical fast Fourier transform processing, Nature Photonics, June 2011; 5(6) 364-371.

[35] Okamoto, K. Fundamentals of Optical Waveguides. Academic Press, San-Diego, USA: Academic Press; 2000.